Journal of Materials Chemistry

Cite this: J. Mater. Chem., 2012, 22, 9173

www.rsc.org/materials

PAPER

Impact of dye end groups on acceptor–donor–acceptor type molecules for solution-processed photovoltaic cells†

Guangrui He,[a] Zhi Li,[a] Xiangjian Wan,[a] Yongsheng Liu,[a] Jiaoyan Zhou,[a] Guankui Long,[a] Mingtao Zhang[b] and Yongsheng Chen*[a]

Received 11th January 2012, Accepted 10th March 2012
DOI: 10.1039/c2jm30194f

Two new oligothiophene derivatives of the acceptor–donor–acceptor type, incorporating double rhodanine or 1,3-dimethylpyrimidine-2,4,6(1*H*,3*H*,5H)-trione units as the terminal acceptor groups, D2R(8 + 2)7T and DTDMP7T, have been designed and synthesized for solution-processable small molecule BHJ solar cells. The impacts of these different end dye moieties on their optical, electrochemical properties, morphology, mobility and solar cell performance were studied. Both compounds exhibit broad and highly efficient solar absorption with low bandgaps of 1.70 and 1.62 eV for D2R(8 + 2)7T and DTDMP7T, respectively. The D2R(8 + 2)7T and DTDMP7T based BHJ solar cell devices achieved a PCE of 2.46% and 4.05%, respectively, under the illumination of AM.1.5, 100 mW cm^{-2}.

Introduction

In recent years, polymer solar cells (PSCs) comprised of a bulk heterojunction (BHJ) layer using polymers as the donors have attracted significant attention due to their ease of synthesis, potential to enable low-cost manufacturing and capability to fabricate flexible large-area devices.[1–4] Power conversion efficiencies (PCEs) of 6–8% have been achieved due to tremendous efforts devoted to designing ideal donor[5–12] and acceptor[13–16] materials and controlling the active layer morphology.[17–19] However, polymer donor materials always suffer from batch-to-batch variations, difficulty of purification, and broad molecular weight distributions.

To overcome these issues, solution-processed small molecules for BHJ organic solar cells (OSCs), combining the advantages of high purity, well defined structure and molecular weight, and no batch-to-batch variations, have stimulated more and more attention.[20–22] So far, significant progress has been made and PCEs of 4–6% have been achieved for OSCs.[23–33] In addition to improving the device fabrication process, an important strategy to improve the performance of OSCs is to design and synthesize new molecules with low band gaps with broad and efficient optical absorption, matched energy levels and high mobility.

Previously, we have reported several molecules using oligothiophene as the backbone with different end groups.[23,34] One example is the compound DCAO7T (Scheme 1) with alkyl cyanoacetate as the electron-withdrawing end group, which offers

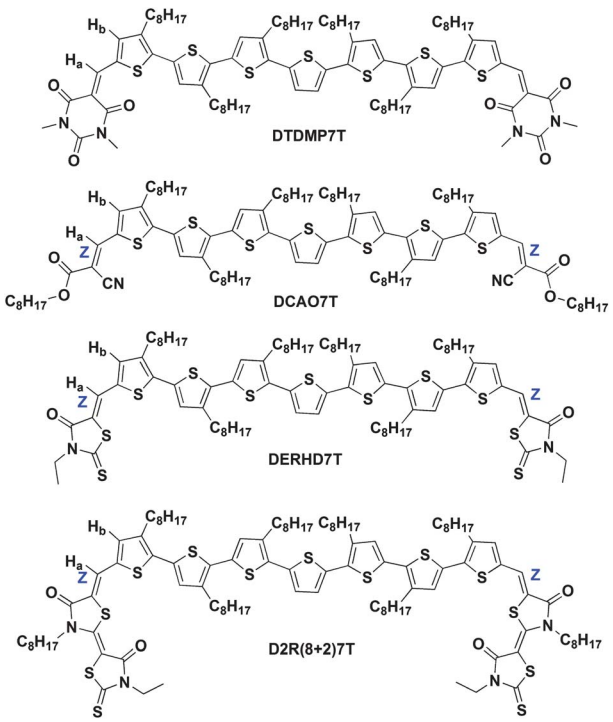

Scheme 1 The chemical structures of DCAO7T, DERHD7T, D2R(8 + 2)7T and DTDMP7T.

[a]*Key Laboratory for Functional Polymer Materials and Centre for Nanoscale Science and Technology, Institute of Polymer Chemistry, College of Chemistry Nankai University, Tianjin 300071, China. E-mail: yschen99@nankai.edu.cn; xjwan@nankai.edu.cn; Fax: +86-(22)-2349-9992*

[b]*Computational Center for Molecular Science Nankai University, Tianjin 300071, China*

† Electronic supplementary information (ESI) available: ^{1}H NMR, ^{13}C NMR, MS and other details. See DOI: 10.1039/c2jm30194f

an encouraging PCE of 5.08%.[23] These molecules indeed demonstrated some advantages. Firstly, they have 6–10 effective conjugated units, resulting in similar solar cell absorption to that for the corresponding polymers. Furthermore, for such an acceptor–donor–acceptor (A–D–A) molecular architecture, the central donor moiety based on the conjugated oligothiophene backbone generally could offer a high mobility, and the side alkyl groups can make the compounds have good solubility and more importantly good film quality using spin-coating.[35] The D–A structure also affords a low band gap resulting from intramolecular charge transfer.[36] In addition, the highest occupied molecular orbital (HOMO) and lowest unoccupied molecular orbital (LUMO) energy levels can also be tuned through designing different backbones, side and end groups, *etc.*[37]

Recently, to improve the light absorption, we introduced a rhodanine unit into the thiophene backbone, forming the targeted OSC molecule DERHD7T (Scheme 1).[30] This molecule gives a much improved short circuit current density (J_{sc}) than that of DCAO7T and thus a significantly higher PCE (6.10%).

Though significant progress has been made for OSCs and PCEs over 6% have been achieved, they are still behind the performance of their corresponding polymers and there is a long way to meet the practical application need. With careful comparison of the three key factors, open circuit voltage (V_{oc}), J_{sc} and fill factor (FF) of the devices based on these small molecules and the corresponding polymers, it can be seen that the J_{sc} for OSCs is the parameter which is most behind that of polymer solar cells, while the other two factors are getting closer to the values of the polymer ones. So, one clear strategy to improve OSC performance is to have better solar light absorption, particularly in the high wavelength range, while the other advantages of these small molecules could be kept simultaneously.

With this strategy in mind, we have designed and synthesized two molecules with two dye end units (Scheme 1), (*E*)-3-ethyl-5-(3-octyl-4-oxothiazolidin-2-ylidene)-2-thioxothiazolidin-4-one (D2R(8 + 2)) and 1,3-dimethylpyrimidine-2,4,6(1*H*,3*H*,5*H*)-trione as the end acceptor moiety to replace the alkyl cyanoacetate terminal in DCAO7T. These acceptor units, with high electron affinities, have been reported to be chromophores with strong optical absorption.[38–45] As expected, these materials indeed show broad and efficient sunlight harvesting owing to their smaller bandgaps. OSC devices were fabricated using these compounds as donors and $PC_{61}BM$ as the acceptor. A PCE of 2.46% was achieved with a V_{oc} of 0.92 V, J_{sc} of 6.77 mA cm^{-2} and a FF of 0.39 for D2R(8 + 2)7T, and a PCE of 4.05% was achieved with a V_{oc} of 0.90 V, J_{sc} of 7.54 mA cm^{-2} and a FF of 0.60 for DTDMP7T. The unexpected low PCEs of these compounds is believed to be due to their lower hole mobilities.

Experimental

Materials

All reactions and manipulations were carried out under argon atmosphere with the use of standard Schlenk techniques. All starting materials, unless otherwise specified, were purchased from commercial suppliers and used without further purification. Diformylseptithiophene (DF7T) (5,5′′′′′′-diformyl-3,3′,3′′,3′′′,3′′′′,3′′′′′-sexioctyl-2,5′:2′,5′′:2′′,2′′′:5′′′,2′′′′:5′′′′,2′′′′′:5′′′′′:2′′′′′′-septithiophene)[46] and 2R(8 + 2) were prepared according to the literature.[47–49]

Instruments and measurements

Nuclear magnetic resonance (NMR) spectra were taken on a Bruker AV400 Spectrometer. MALDI-TOF spectra were performed on a Bruker Autoflex III instrument. The thermogravimetric analyses (TGA) was carried out on a NETZSCH STA 409PC instrument under nitrogen gas flow with a 10 °C min^{-1} heating rate. UV–Vis spectra were obtained with a JASCO V-570 spectrophotometer. The organic molecule films on quartz used for absorption spectral measurement were prepared by spin-coating their chloroform solutions. X-Ray diffraction (XRD) experiments were performed on a Rigaku D/max-2500 X-ray diffractometer with Cu-Kα radiation (k = 1.5406 Å) at a generator voltage of 40 kV and a current of 100 mA. Cyclic voltammetry (CV) experiments were performed with a LK98B II microcomputer-based electrochemical analyzer in CH_2Cl_2 solutions. All measurements were carried out at room temperature with a conventional three-electrode configuration employing a glassy carbon electrode as the working electrode, a saturated calomel electrode (SCE) as the reference electrode, and a Pt wire as the counter electrode. Dichloromethane was distilled from calcium hydride under dry nitrogen immediately prior to use. Tetrabutylammonium phosphorus hexafluoride (Bu_4NPF_6, 0.1 M) in dichloromethane was used as the supporting electrolyte, and the scan rate was 100 mV s^{-1}.

Hole mobility was measured according to a similar method described in the literature,[50,51] using a diode configuration of ITO/PEDOT:PSS/D2R(8 + 2)7T or DTDMP7T/Al by taking a dark current in the range of 0–8 V and fitting the results to a space charge limited form, where the SCLC is described by

$$J = 9\varepsilon_0\varepsilon_r\mu_h V^2/8L^3$$

where J is the current density, L is the film thickness of active layer, μ_h is the hole mobility, ε_r is the relative dielectric constant of the transport medium, ε_0 is the permittivity of free space (8.85×10^{-12} F m^{-1}), V is the internal voltage in the device and $V = V_{appl} - V_r - V_{bi}$, where V_{appl} is the applied voltage to the device, V_r is the voltage drop due to contact resistance and series resistance across the electrodes, and V_{bi} is the built-in voltage due to the relative work function difference of the two electrodes.

Fabrication and characterization of organic solar cells

The photovoltaic devices were fabricated with a structure of glass/ITO/PEDOT:PSS/donor:acceptor/LiF or Ca/Al. The ITO-coated glass substrates were cleaned by ultrasonic treatment in detergent, deionized water, acetone, and isopropyl alcohol under ultrasonication for 15 min each and subsequently dried by a nitrogen blow. A thin layer of PEDOT:PSS (Baytron P VP AI 4083, filtered at 0.45 μm) was spin-coated (4000 rpm, *ca.* 40 nm thick) onto the ITO surface. After being baked at 150 °C for 20 min, the substrates were transferred into an argon-filled glove box. Subsequently, the active layer was spin-coated from different blend ratios (weight-to-weight) of donor (8 mg mL^{-1}) and $PC_{61}BM$ in chloroform solution at 1500 rpm for 20 s on the

ITO/PEDOT:PSS substrate without any further special treatments. The active layer thickness was measured using a Dektak 150 profilometer. Finally, a ~1 nm LiF or 20 nm Ca layer and a 80 nm Al layer were deposited on the active layer under high vacuum (<3 × 10^{-4} Pa). The effective area of each cell was 4 mm^2, defined by masks for all the solar cell devices discussed in this work.

The current density–voltage (*J–V*) curves of the photovoltaic devices were obtained by a Keithley 2400 source-measure unit. The photocurrent was measured under simulated illumination at 100 mW cm^{-2} AM 1.5G irradiation using a xenon-lamp-based solar simulator (Oriel 96000 (AM 1.5G)) in an argon filled glove box. The simulator irradiance was calibrated using a certified silicon diode.

Synthesis

The synthesis routes to D2R(8 + 2)7T and DTDMP7T are shown in Scheme 2.

2R(8 + 2). To an acetonitrile solution (30 ml) of 3-ethylrhodanine (2.92 g, 18 mmol) and isothiocyanate (2.79 g, 18 mmol) was added 1,8-diazabicyclo (5,4,0) undec-7-ene (DBU) (2.74 g, 18 mmol) at room temperature. The mixture was stirred for 30 min. Then, to the mixture was added ethyl bromoacetate (6.01 g, 36 mmol). The mixture was stirred for 30 min and then refluxed for 4 h. After the reaction was completed, the mixture was concentrated and dissolved in chloroform. Aqueous 2 M hydrochloric acid (100 ml) was added to the mixture, and the pH was adjusted to below 3. The product was extracted with chloroform and dried over Na_2SO_4. After removal of the solvent, the crude product was chromatographed on silica gel using a mixture of dichloromethane and petroleum ether (1 : 1) as eluent to afford 2R(8 + 2) as a primrose solid (4.69 g, 70% yield). ^{1}H NMR (400 MHz, $CDCl_3$): δ 4.17(q, J = 6.8, 2H), 3.85 (t, J = 6.0, 2H), 3.82 (s, 2H), 1.60–1.70 (m, 2H), 1.22–1.45 (m, 13H), 0.89 (s, 3H). ^{13}C NMR (400 MHz, $CDCl_3$): δ 189.945, 172.888, 167.405, 151.496, 93.710, 44.980, 39.845, 31.696, 31.507, 29.391, 29.068, 26.369, 22.606, 14.085, 12.137. MS (MALDI-TOF) *m/z*: calcd for $C_{16}H_{24}N_2O_2S_3$ $[M]^+$, 372.10; found, 372.08.

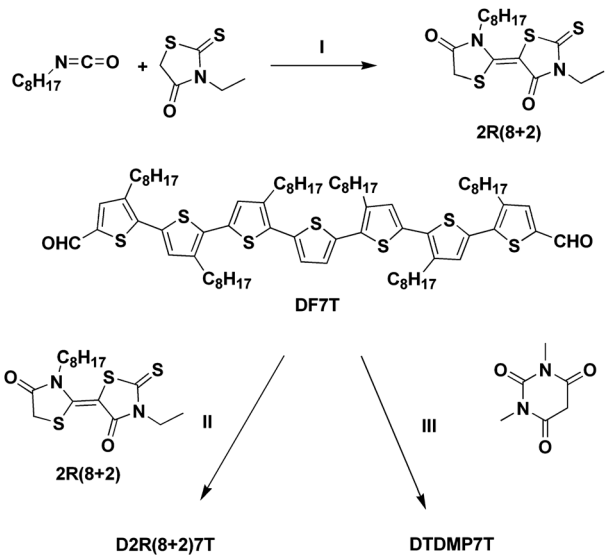

Scheme 2 Synthesis routes to the compounds: (I) (1) CH_3CN, DBU, room temperature for 30 min; (2) $BrCH_2COOEt$, reflux for 4 h; (II) acetic acid, chlorobenzene, ammonium acetate, Ar, reflux overnight; (III) $CHCl_3$, triethylamine, Ar, room temperature for 20 h.

D2R(8 + 2)7T. To an acetic acid and chlorobenzene mixture solution (60 ml, v : v = 2 : 1) containing 2R(8 + 2) (356 mg, 1.00 mmol) and DF7T (13 mg, 0.10 mmol) was added ammonium acetate (77 mg,1 mmol). Under argon, the mixture was stirred and refluxed overnight. The reaction mixture was poured into water, then extracted with CH_2Cl_2, washed with water and dried over Na_2SO_4. After removal of the solvent, the crude product was chromatographed on silica gel using a mixture of dichloromethane and petroleum ether (1 : 1) as eluent to afford D2R(8 + 2)7T as a dark blue solid (140 mg, 70% yield). ^{1}H NMR (400 MHz, $CDCl_3$): δ 7.76 (s, 2H), 7.18 (s, 2H), 7.13 (s, 2H), 7.11 (s, 2H), 7.02 (s, 2H), 4.19 (q, J = 7.2, 4H), 3.94 (t, J = 8.0, 4H), 2.72–2.90 (m, 12H), 1.64–1.80 (m, 16H), 1.22–1.50 (m, 86H), 0.84–0.94 (m, 24H). ^{13}C NMR (400 MHz, $CDCl_3$): δ 189.443, 166.962, 166.540, 145.491, 140.812, 140.211, 140.018, 139.367, 137.280, 135.712, 134.853, 133.425, 132.657, 132.373, 130.853, 130.037, 128.856, 125.940, 117.401, 93.804, 45.258, 39.934, 31.946, 31.756, 30.647, 30.217, 29.738, 29.542, 29.483, 29.457, 29.386, 29.137, 26.485, 22.717, 22.652, 14.149, 12.256. MS (MALDI-TOF) *m/z*: calcd for $C_{110}H_{156}N_4O_4S_{13}$ $[M]^+$, 2013.85; found, 2013.83.

DTDMP7T. Diformylseptithiophene (DF7T) (130 mg, 0.10 mmol) was dissolved in a solution of dry $CHCl_3$ (50 mL) and three drops of triethylamine and then 1,3-dimethylpyrimidine-2,4,6(1*H*,3*H*,5*H*)-trione (156 mg, 1.00 mmol) was added and the resulting solution was stirred for 20 h, under argon, at room temperature. The reaction mixture was poured into water, then extracted with CH_2Cl_2, washed with water and dried over Na_2SO_4. After removal of the solvent, the product was chromatographed on silica gel using a mixture of dichloromethane and petroleum ether as eluent to afford DTDMP7T as a black solid (120 mg, 79% yield). ^{1}H NMR (400 MHz, $CDCl_3$): δ 8.56 (s, 2H), 7.66 (s, 2H), 7.35 (s, 2H), 7.13 (s, 2H), 7.05 (s, 2H), 3.43 (d, 12H), 2.70–2.90 (m, 12H), 1.66–1.77 (m, 12H), 1.24–1.48 (m, 60H), 0.88 (t, J = 6.4 Hz, 18H). ^{13}C NMR (400 MHz, $CDCl_3$): δ 162.836, 162.096, 151.475, 148.848, 148.030, 140.562, 140.312, 140.249, 135.746, 134.171, 133.813, 133.271, 132.622, 131.347, 131.234, 129.254, 126.194, 108.769, 31.913, 30.625, 30.541, 29.934, 29.710, 29.639, 29.429, 29.283, 28.884, 28.147, 22.698, 14.131. MS (MALDI-TOF) *m/z*: calcd for $C_{90}H_{124}N_4O_6S_7$ $[M]^+$, 1580.76; found, 1580.71.

Results and discussion

Synthesis and thermal stability of the compounds

D2R(8 + 2)7T and DTDMP7T were synthesized by the routes shown in Scheme 2. (*E*)-3-ethyl-5-(3-octyl-4-oxothiazolidin-2-ylidene)-2-thioxothiazolidin-4-one (D2R(8 + 2)) was prepared according to the literature.[47–49] By the Knoevenagel condensation of compound DF7T with 2R(8 + 2) and 1,3-dimethylpyrimidine-2,4,6(1*H*,3*H*,5*H*)-trione, respectively, the targeted molecules

D2R(8 + 2)7T and DTDMP7T were afforded. The exact configurations of these two molecules, along with our previously reported molecules DCAO7T and DERHD7T, were investigated by ROESY spectrum, ^{1}H NMR spectrum and other methods (see Scheme 1 and supporting information Section B†).

Thermogravimetric analysis (TGA) suggests that D2R(8 + 2)7T and DTDMP7T exhibit good stability with decomposition temperature (T_d) greater than 360 °C under N_2 atmosphere (see Fig. 1).

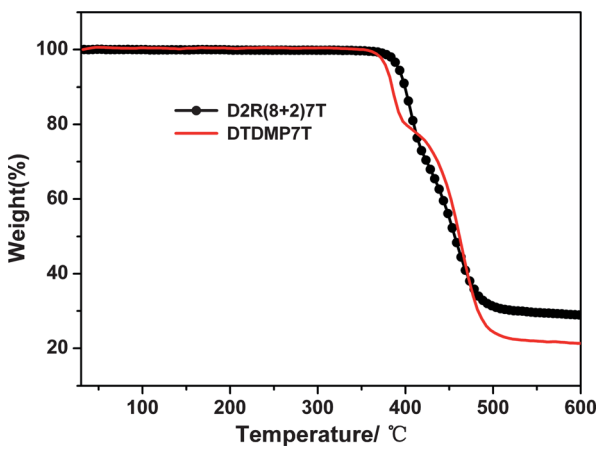

Fig. 1 TGA plot of D2R(8 + 2)7T and DTDMP7T.

Optical absorption

The UV-vis absorption spectra of D2R(8 + 2)7T and DTDMP7T, together with DCAO7T[23] and DERHD7T[30] for comparison, in diluted chloroform solution with a concentration of 10^{-5} mol L^{-1} and that from their films prepared by spin coating are shown in Fig. 2. The important optical absorption data, together with that from electrochemical studies, are summarized in Table 1.

Compared with the absorption peaks at 492 nm of DCAO7T solution and 508 nm of DERHD7T solution, as shown in Fig. 2a, D2R(8 + 2)7T (534 nm) and DERHD7T (537 nm) have a red-shift of about 30–40 nm. In addition, it is noticed that D2R(8 + 2)7T exhibits a more broad absorption with two absorption peaks at 420 and 533 nm than the other molecules.

Also, as shown in Fig. 2b, red shifted absorption maxima were observed at 584 nm for D2R(8 + 2)7T film and 602 nm for the DTDMP7T film, compared with that of DCAO7T (580 nm). The absorption coefficient of these two new compounds, D2R(8 + 2)7T and DTDMP7T, is similar to that of DCAO7T, while DERHD7T has a slightly higher absorption coefficient. The optical band gaps of D2R(8 + 2)7T and DTDMP7T thin films were estimated from the onset of the film absorption spectra to be 1.70 eV and 1.67eV (Table 1), lower than that of the compared compound of DCAO7T. These optical results indicate that, as we designed, the two new compounds, D2R(8 + 2)7T and DTDMP7T, could match better with sunlight in terms of spectrum than that of DCAO7T.[23]

The absorption spectra of these compounds in the film state (Fig. 2b) show an obvious broadening and bathochromic shift of the bands compared to the solution spectra, indicating that these

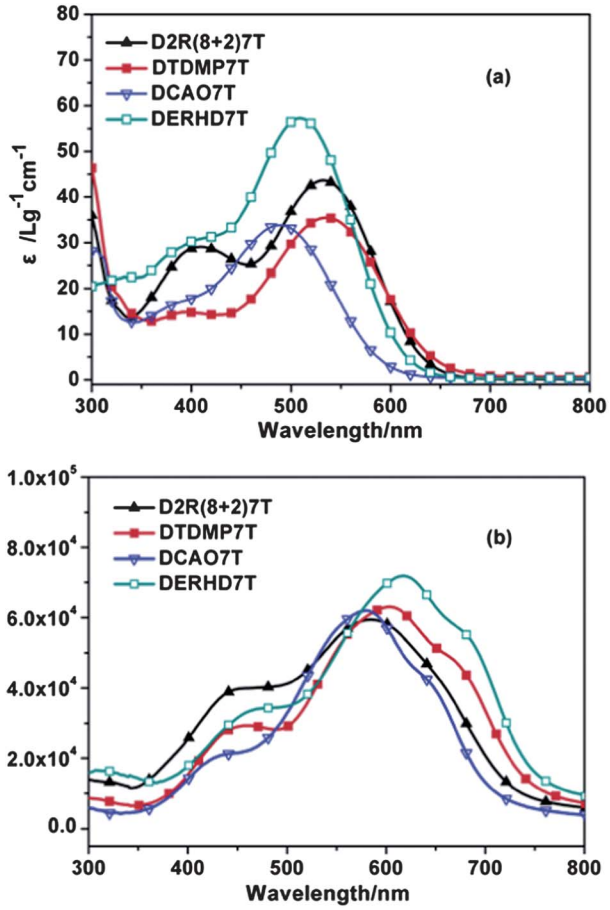

Fig. 2 (a) Absorption spectra of DCAO7T, DERHD7T, D2R(8 + 2)7T and DTDMP7T in chloroform solution; (b) absorption spectra of DCAO7T, DERHD7T, D2R(8 + 2)7T and DTDMP7T as films.

molecules all follow *J* aggregates in the film state.[52] In comparison with the solution, the film absorption peaks of D2R(8 + 2)7T and DTDMP7T (see Fig. 2b) are red shifted by 50 nm and 68 nm, respectively, smaller than that of DCAO7T (88 nm) and DERHD7T (110 nm). This means that D2R(8 + 2)7T and DTDMP7T do not have the same efficient packing as DCAO7T and DERHD7T, which will be confirmed in the following XRD results.

Electrochemical properties and electronic energy levels

The electrochemical properties of D2R(8 + 2)7T and DTDMP7T were investigated by cyclic voltammetry (CV). The potentials were internally calibrated using the ferrocene/ferrocenium of the (Fc/Fc^+) redox couple (4.8 eV below the vacuum level). As shown in Fig. 3, the CV of D2R(8 + 2)7T and DTDMP7T in CH_2Cl_2 solution show two reversible oxidation waves and one irreversible reduction wave. The energy levels of the HOMO and LUMO, which are −5.09 and −3.39 eV for D2R(8 + 2)7T, and −5.12 and −3.50 eV for DTDMP7T, were calculated from the onset oxidation potential and the onset reduction potential. The values of the bandgaps, HOMO and LUMO energy levels of the two compounds, along with those of DCAO7T and DERHD7T for comparison,[23,30] were listed in Table 1. From

Table 1 Optical and electrochemical data of the molecules DCAO7T, DERHD7T, D2R(8 + 2)7T and DTDMP7T

Compounds	λ_{max} solution/nm	ε solution/ L g^{-1}cm^{-1}	λ_{max} film/nm	ε film/cm^{-1}	(E_g^{opt})film/eV	E_g^{cv}/eV	HOMO/eV	LUMO/eV
D2R(8 + 2)7T	534	44	584	6.0×10^4	1.70	1.70	−5.09	−3.39
DTDMP7T	537	35	605	6.3×10^4	1.67	1.62	−5.12	−3.50
DCAO7T[a]	492	34	580	6.2×10^4	1.74	1.84	−5.13	−3.29
DERHD7T[b]	508	56	618	7.2×10^4	1.69	1.72	−5.00	−3.28

[a] Data from ref. 23. [b] Data from ref. 30.

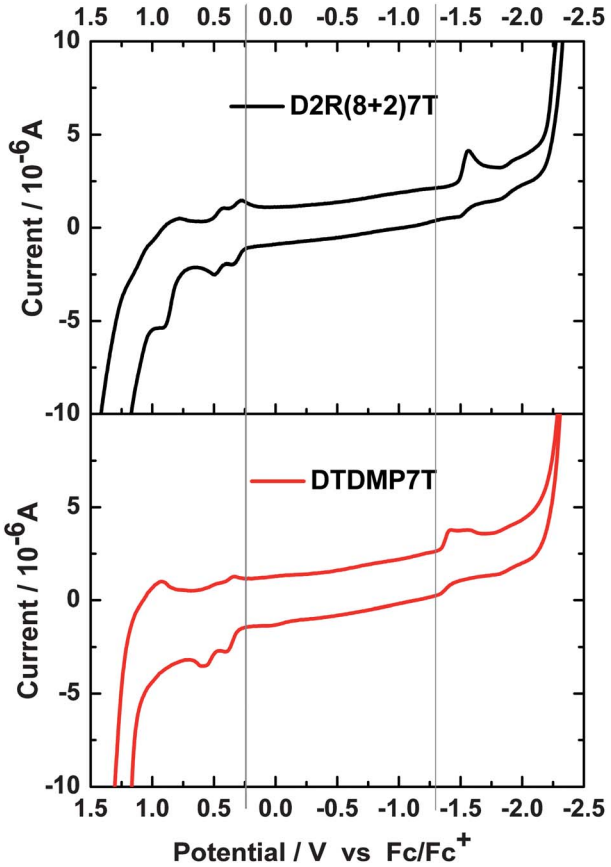

Fig. 3 Cyclic voltammograms of D2R(8 + 2)7T and DTDMP7T films on Pd/C electrode in an dichloromethane solution of 0.1 mol L^{-1} Bu_4NPF_6 with a scan rate of 100 mV s^{-1}.

Table 1, we can see that the HOMO energy levels of these molecules are very similar (~−5.10 eV), which is predominantly determined by the donor moiety (oligothiophene unit). Different from the HOMO, the electrochemical band gap, 1.70 eV for D2R(8 + 2)7T and 1.62 eV for DTDMP7T, compared with that of DCAO7T (1.84 eV) and DERHD7T (1.72 eV). These results are consistent with those from optical data and demonstrate that the band gap of this kind of molecule can be tuned effectively through the introduction of different acceptor terminal units as we discussed earlier.

X-Ray diffraction (XRD) and structure calculations

The structural ordering of pristine D2R(8 + 2)7T and DTDMP7T was investigated by X-ray diffraction (XRD) analysis for the films spin-coated from $CHCl_3$ solutions onto glass substrates. The XRD patterns of the D2R(8 + 2)7T and DTDMP7T films, together with that of DCAO7T[23] and DERHD7T,[30] are shown in Fig. 4.

From Fig. 4, we can see that no clear reflection peak was observed for D2R(8 + 2)7T, indicating that poor stacking of the donor molecule was formed in the spin-coating procedure for this molecule. For DTDMP7T, a moderate intensity (100) reflection peak at $2\theta = 4.6°$, corresponding to a d_{100}-spacing value of 19.0 Å was observed. The d_{100}-spacing value is the distance between the planes of the main conjugation chains of the molecules separated by alkyl side chains. The second-order diffraction peak (200) and the third-order diffraction peak (300) were not observed. The XRD results are significantly different from those of the two previous molecules, DCAO7T and DERHD7T, as shown in Fig. 4.

This clearly indicates that in contrast to the molecules DCAO7T and DERHD7T, these two new molecules do not form

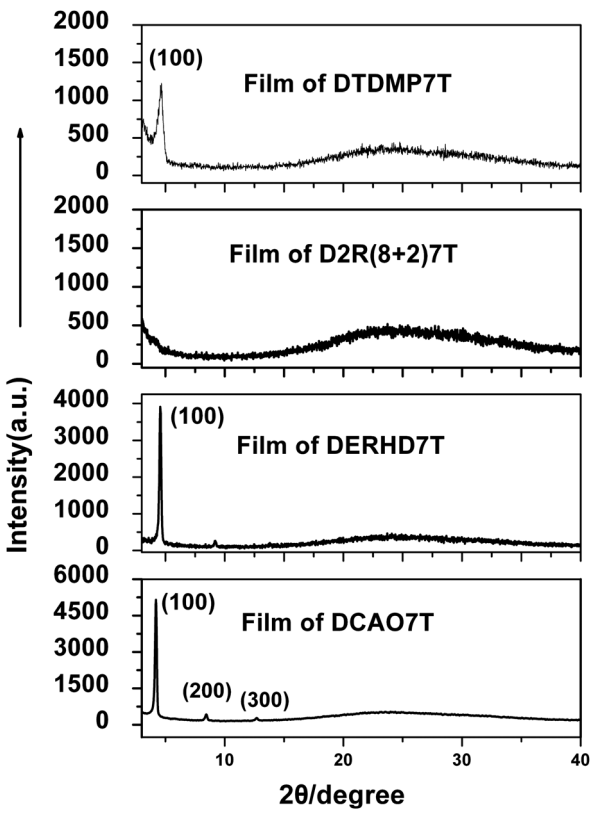

Fig. 4 XRD patterns of DCAO7T, DERHD7T, D2R(8 + 2)7T and DTDMP7T films spin-coated from $CHCl_3$ onto glass substrate.

a well ordered packing morphology in solid state. Furthermore, the XRD of the blended films of these two molecules with $PC_{61}BM$ have similar patterns to their pristine XRD (Fig. S3†).

In order to further understand the morphological performances of these two molecules, the optimized geometrical structures of D2R(8 + 2)7T and DTDMP7T were investigated using density functional theory (DFT) with the Gaussian 09 program, and the optimized geometry was shown in Fig. S1 and Fig. S2.†[53] Note in the optimized structure that the *n*-octyl group substituted onto the rhodanine ring is not coplanar with the conjugated backbone of the molecule, which could disturb the stacking of the D2R(8 + 2)7T molecules in the solid state. For DTDMP7T, the molecule has a coplanar structure, however, the stacking of the molecules in the film is not as good compared with that of DCAO7T and DERHD7T, which may be due to the acceptor unit not being in a straight line with the oligothiophene backbone. These modelling results are consistent with those from the XRD data.

Morphology of the donor:$PC_{61}BM$ blend films

The morphology of the photoactive layer is one of the key factors determining the photovoltaic performance of OSCs.[54,55] We used atomic force microscopy (AFM) to investigate the morphology of the two organic molecules:$PC_{61}BM$ blend films. These blend films were prepared by spin-coating their chloroform solutions on top of the PEDOT:PSS layer, which was spin-coated on ITO glass.

As shown in Fig. 5, the roughness (rms) of the blend films is 1.03 and 3.96 nm for the D2R(8 + 2)7T/$PC_{61}BM$ and DTDMP7T/$PC_{61}BM$ films, respectively, comparable to that of DCAO7T (0.38 nm) and DERHD7T (7.76 nm) films blended with $PC_{61}BM$.[23,30] We can see that the surfaces of these two films are smooth and uniform, indicating that the replacement of the end group with two new dye end units does not change the compound film quality.

Hole mobility

The hole mobility of the pristine D2R(8 + 2)7T and DTDMP7T films was measured by the space charge limited current (SCLC) method. As plotted in Fig. S7† and listed in Table 2, the D2R(8 + 2)7T and DTDMP7T films show hole mobilities of 2.4×10^{-5} cm^2 V^{-1} s^{-1} and 4.7×10^{-5} cm^2 V^{-1} s^{-1}, respectively, which are significantly lower than those for DCAO7T (3.26×10^{-4} cm^2 V^{-1} s^{-1}) and DERHD7T (1.50×10^{-4} cm^2 V^{-1} s^{-1}).[23,30] These smaller hole mobilities are probably due to the poor packing of the donors in the films, as observed from the XRD data above.

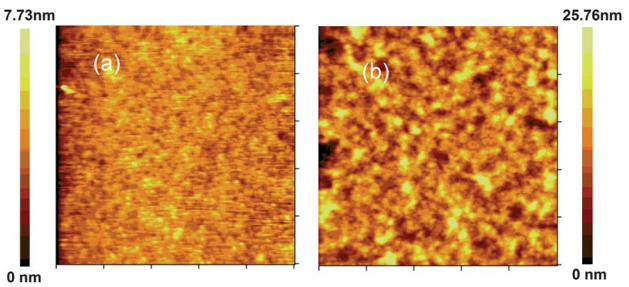

Fig. 5 AFM images of the molecule:$PC_{61}BM$ films spin-coated from their solutions at a weight ratio of (1 : 0.5) for D2R(8 + 2)7T and (1 : 0.8) for DTDMP7T: (a) D2R(8 + 2)7T:$PC_{61}BM$ film, (b) DTDMP7T:$PC_{61}BM$ film, the scan size of the images is 5 μm × 5 μm.

Photovoltaic performance

Bulk-heterojunction OSCs were fabricated by using the two new organic molecules as the donor materials, and $PC_{61}BM$ as the acceptor material, using the conventional solution spin-coating process. The device structure is ITO/PEDOT:PSS/photoactive layer/Ca/Al. Device optimizations were conducted by varying the weight ratios of donor *vs.* acceptor (summarized in Table S2 and shown in Fig. S4 and Fig. S5†). The optimal typical current density–voltage (*J*–*V*) curves of the OSCs were shown in Fig. 6 and the optimal results were summarized in Table 2.

For D2R(8 + 2)7T, the optimal efficiency was obtained from the device with the active layer comprised of a blend of D2R(8 + 2)7T and $PC_{61}BM$ with a weight ratio of 1 : 0.5 and an optimized thickness of about 80 nm. This OSC device gave an open circuit voltage (V_{oc}) of 0.92 V, a short circuit current density (J_{sc}) of 6.77 mA cm^{-2}, a fill factor (FF) of 0.39 and a PCE of 2.46%. The optimal OSC device based on the DTDMP7T:$PC_{61}BM$ (1 : 0.8, w/w) blend showed a V_{oc} of 0.90 V, a J_{sc} of 7.54 mA cm^{-2}, a FF of 0.60 and a PCE of 4.05%.

During our optimization, LiF/Al instead of Ca/Al as the cathode was also investigated. The device of DTDMP7T/$PC_{61}BM$ with the same ratio of 1 : 0.8 displayed a significantly lower PCE of 2.07% with a FF of 0.39. Similar results were observed for the D2R(8 + 2)7T based device (Fig. S6 supporting information†). The lower FF and lower PCE for devices with a LiF/Al cathode could be ascribed to the interfacial contact issue between the active layer and the electrode.[56,57]

From Fig. 6 and Table 2, we can see that the characteristically high open circuit voltages (V_{oc}) of the devices based on D2R(8 + 2)7T and DTDMP7T (0.92 V and 0.90 V, respectively), are similar to those of DCAO7T (0.86 V) and DERHD7T (0.92 V). Thus, the V_{oc} is typically high because the HOMO energy levels of these molecules, predominantly determined by the backbone donor moiety, change little when different dye end groups were introduced. To some extent, we can infer that a high V_{oc} can always be maintained for this kind of molecule with different dye end groups.

On the other hand, the lower photocurrent J_{sc} of the two new molecules leads to relatively lower efficiencies for the OSC devices. In order to further understand the device performance, the external quantum efficiency (EQE) of these two molecule based devices was measured as shown in Fig. 7. From the curves, we can see that the D2R(8 + 2)7T and DTDMP7T based devices, along with DERHD7T, show broader absorption regions than DCAO7T. However, the EQE values of the D2R(8 + 2)7T and DTDMP7T based devices are all below 40% from 350 to 750 nm, much lower than those of DCAO7T and DERHD7T (about 60–70%). The two factors above together determine that DERHD7T based OSCs have the highest photocurrent, while these two new molecule based OSCs exhibit a relatively low photocurrent.

The lower EQE values of these two new molecule based devices indicate that the photoresponse of these two molecules

Table 2 Current density–voltage characteristics of the OSC devices based on the blend of D2R(8 + 2)7T (1 : 0.5, w/w) or DTDMP7T/$PC_{61}BM$ (1 : 0.8, w/w) under the illumination of AM.1.5, 100 mW cm^{-2}. The device structure is ITO/PEDOT:PSS/photoactive layer/Ca/Al. (expect for DERHD7T based devices using LiF/Al as cathode)

Active layer	V_{oc}/V	J_{sc}/mA cm^{-2}	FF	PCE (%)	μ_h/cm^2 V^{-1} s^{-1} ($\times 10^{-4}$)
DCAO7T:$PC_{61}BM$[a]	0.86	10.74	0.55	5.08	3.26
DERHD7T:$PC_{61}BM$[b]	0.92	13.98	0.47	6.10	1.50
D2R(8 + 2)7T:$PC_{61}BM$	0.92	6.77	0.39	2.46	0.24
DTDMP7T:$PC_{61}BM$	0.90	7.54	0.60	4.05	0.47

[a] Data from ref. 23. [b] Data from ref. 30.

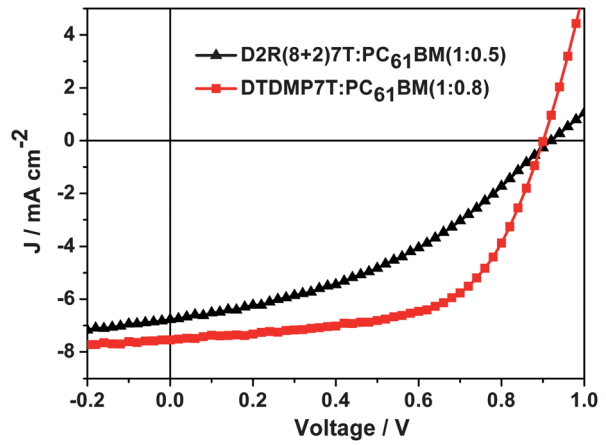

Fig. 6 Current density–voltage characteristics of the OSC devices based on the blend of D2R(8 + 2)7T or DTDMP7T/$PC_{61}BM$ (w/w) under the illumination of AM.1.5, 100 mW cm^{-2}.

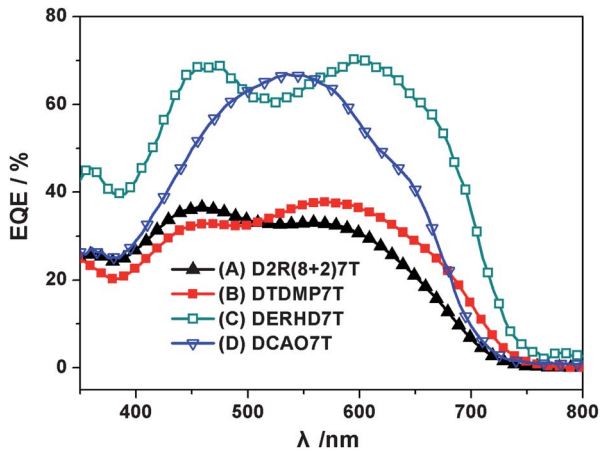

Fig. 7 EQE of (A) D2R(8 + 2)7T:$PC_{61}BM$ (1 : 0.5), (B) DTDMP7T:$PC_{61}BM$ (1 : 0.8), (C) DERHD7T:$PC_{61}BM$ (1 : 0.5) (D) DCAO7T:$PC_{61}BM$ (1 : 0.5) active layer OPV devices. EQE spectra were measured using a QEW7 Solar Cell QE measurement system (PV Measurements).

are not efficient in the BHJ devices. The external quantum efficiency (EQE) can be represented by the product of each efficiency in the following fundamental processes: light absorption (η_A), exciton diffusion (η_{ED}), charge dissociation (η_{CD}), charge transfer (η_{CT}) and charge collection at the electrodes (η_{CC}).[58] At present, we cannot evaluate how these different acceptor units impact on each fundamental processes of EQE. However, we can infer that the stacking mold of the donors plays a key role in the charge collection efficiency and the EQE. For these two new molecules, the lower EQE are closely related to the poorer packing in the OSC devices.

Conclusions

Two new end dye moieties as the acceptor units-double rhodanine 2R(8 + 2) and 1,3-dimethylpyrimidine-2,4,6(1*H*,3*H*,5*H*)-trione, were introduced to the oligothiophene based donor unit, forming two A–D–A type molecules D2R(8 + 2)7T and DTDMP7T. As expected, the bandgaps of these two compounds are lower than those of DCAO7T and DERHD7T, indicating that the band gaps and energy levels of these small molecules can be tuned through changing the terminal group. In addition, the terminal acceptor groups of these small molecules also play a great role in their packing mold in the solid state, which has a great impact on their hole mobility. The poor packing in the solid state of these two molecules offers a lower hole mobility, which leads to relatively lower PCEs of 2.46% and 4.05% for D2R(8 + 2)7T and DTDMP7T, respectively, under the illumination of AM.1.5, 100 mW cm^{-2}. These results indicate that the balanced consideration of absorption, morphology, mobility, solubility, *etc.* for the dedicated design of small molecule OSCs and systematic investigations are highly needed to improve the overall OSC performance.

Acknowledgements

The authors gratefully acknowledge financial support from the NSFC (grants 50933003, 50902073 and 50903044), MOST (grants 2012CB933401 and 2011DFB50300) and NSF of Tianjin City (grant 10ZCGHHZ00600).

Notes and references

1 A. C. Arias, J. D. MacKenzie, I. McCulloch, J. Rivnay and A. Salleo, *Chem. Rev.*, 2010, **110**, 3.
2 L. M. Chen, Z. R. Hong, G. Li and Y. Yang, *Adv. Mater.*, 2009, **21**, 1434.
3 A. J. Heeger, *Chem. Soc. Rev.*, 2010, **39**, 2354.
4 R. Po, M. Maggini and N. Camaioni, *J. Phys. Chem. C*, 2010, **114**, 695.
5 H. Y. Chen, J. Hou, S. Zhang, Y. Liang, G. Yang, Y. Yang, L. Yu, Y. Wu and G. Li, *Nat. Photonics*, 2009, **3**, 649.
6 T. Y. Chu, J. Lu, S. Beauprell, Y. Zhang, J.-R. Pouliot, S. Wakim, J. Zhou, M. Leclerc, Z. Li, J. Ding and Y. Tao, *J. Am. Chem. Soc.*, 2011, **133**, 4250.
7 J. Hou, H. Y. Chen, S. Zhang, R. I. Chen, Y. Yang, Y. Wu and G. Li, *J. Am. Chem. Soc.*, 2009, **131**, 15586.

8 Y. Y. Liang, Z. Xu, J. B. Xia, S. T. Tsai, Y. Wu, G. Li, C. Ray and L. P. Yu, *Adv. Mater.*, 2010, **22**, E135.
9 C. Piliego, T. W. Holcombe, J. D. Douglas, C. H. Woo, P. M. Beaujuge and J. M. J. Fréchet, *J. Am. Chem. Soc.*, 2010, **132**, 7595.
10 S. C. Price, A. C. Stuart, L. Yang, H. Zhou and W. You, *J. Am. Chem. Soc.*, 2011, **133**, 4625.
11 H. Zhou, L. Yang, A. C. Stuart, S. C. Price, S. Liu and W. You, *Angew. Chem., Int. Ed.*, 2011, **50**, 2995.
12 Z. He, C. Zhong, X. Huang, W.-Y. Wong, H. Wu, L. Chen, S. Su and Y. Cao, *Adv. Mater.*, 2011, **23**, 4636.
13 Y. He, H. Y. Chen, J. Hou and Y. Li, *J. Am. Chem. Soc.*, 2010, **132**, 1377.
14 Y. He, G. Zhao, B. Peng and Y. Li, *Adv. Funct. Mater.*, 2010, **20**, 3383.
15 G. Zhao, Y. He and Y. Li, *Adv. Mater.*, 2010, **22**, 4355.
16 G. Zhao, Y. He, Z. Xu, J. Hou, M. Zhang, J. Min, H. Y. Chen, M. Ye, Z. Hong, Y. Yang and Y. Li, *Adv. Funct. Mater.*, 2010, **20**, 1480.
17 C. J. Brabec, M. Heeney, I. McCulloch and J. Nelson, *Chem. Soc. Rev.*, 2011, **40**, 1185.
18 A. J. Moule and K. Meerholz, *Adv. Mater.*, 2008, **20**, 240.
19 J. Peet, A. J. Heeger and G. C. Bazan, *Acc. Chem. Res.*, 2009, **42**, 1700.
20 M. T. Lloyd, J. E. Anthony and G. G. Malliaras, *Mater. Today*, 2007, **10**, 34.
21 J. Roncali, *Acc. Chem. Res.*, 2009, **42**, 1719.
22 B. Walker, C. Kim and T. Q. Nguyen, *Chem. Mater.*, 2011, **23**, 470.
23 Y. Liu, X. Wan, F. Wang, J. Zhou, G. Long, J. Tian, J. You, Y. Yang and Y. Chen, *Adv. Energy Mater.*, 2011, **1**, 771.
24 S. Loser, C. J. Bruns, H. Miyauchi, R. o. P. Ortiz, A. Facchetti, S. I. Stupp and T. J. Marks, *J. Am. Chem. Soc.*, 2011, **133**, 8142.
25 Y. Matsuo, Y. Sato, T. Niinomi, I. Soga, H. Tanaka and E. Nakamura, *J. Am. Chem. Soc.*, 2009, **131**, 16048.
26 H. Shang, H. Fan, Y. Liu, W. Hu, Y. Li and X. Zhan, *Adv. Mater.*, 2011, **23**, 1554.
27 B. Verreet, B. P. Rand, D. Cheyns, A. Hadipour, T. Aernouts, P. Heremans, A. Medina, C. G. Claessens and T. Torres, *Adv. Energy Mater.*, 2011, **1**, 565.
28 B. Walker, A. B. Tamayo, X. D. Dang, P. Zalar, J. H. Seo, A. Garcia, M. Tantiwiwat and T. Q. Nguyen, *Adv. Funct. Mater.*, 2009, **19**, 3063.
29 G. Wei, S. Wang, K. Sun, M. E. Thompson and S. R. Forrest, *Adv. Energy Mater.*, 2011, **1**, 184.
30 Z. Li, G. He, X. Wan, Y. Liu, J. Zhou, G. Long, Y. Zuo, M. Zhang and Y. Chen, *Adv. Energy Mater.*, 2012, **2**, 74.
31 Y. Liu, X. Wan, F. Wang, J. Zhou, G. Long, J. Tian and Y. Chen, *Adv. Mater.*, 2011, **23**, 5387.
32 J. Zhou, X. Wan, Y. Liu, G. Long, F. Wang, Z. Li, Y. Zuo, C. Li and Y. Chen, *Chem. Mater.*, 2011, **23**, 4666.
33 Y. Sun, G. C. Welch, W. L. Leong, C. J. Takacs, G. C. Bazan and A. J. Heeger, *Nat. Mater.*, 2012, **11**, 44.
34 Y. Liu, X. Wan, B. Yin, J. Zhou, G. Long, S. Yin and Y. Chen, *J. Mater. Chem.*, 2010, **20**, 2464.
35 A. Salleo, R. J. Kline, D. M. DeLongchamp and M. L. Chabinyc, *Adv. Mater.*, 2010, **22**, 3812.
36 J. Roncali, *Chem. Rev.*, 1997, **97**, 173.
37 H. Meier, *Angew. Chem., Int. Ed.*, 2005, **44**, 2482.
38 T. Horiuchi, H. Miura, K. Sumioka and S. Uchida, *J. Am. Chem. Soc.*, 2004, **126**, 12218.
39 S. Ito, H. Miura, S. Uchida, M. Takata, K. Sumioka, P. Liska, P. Comte, P. Pechy and M. Gratzel, *Chem. Commun.*, 2008, 5194.
40 S. Ito, S. M. Zakeeruddin, R. Humphry-Baker, P. Liska, R. Charvet, P. Comte, M. K. Nazeeruddin, P. Péchy, M. Takata, H. Miura, S. Uchida and M. Grätzel, *Adv. Mater.*, 2006, **18**, 1202.
41 A. Konno, G. R. A. Kumara, S. Kaneko, B. Onwona-Agyeman and K. Tennakone, *Chem. Lett.*, 2007, **36**, 716.
42 D. Kuang, S. Uchida, R. Humphry-Baker, S. M. Zakeeruddin and M. Grätzel, *Angew. Chem., Int. Ed.*, 2008, **47**, 1923.
43 A. Mishra, M. K. R. Fischer and P. Bäuerle, *Angew. Chem., Int. Ed.*, 2009, **48**, 2474.
44 Q. Li, C. Lu, J. Zhu, E. Fu, C. Zhong, S. Li, Y. Cui, J. Qin and Z. Li, *J. Phys. Chem. B*, 2008, **112**, 4545.
45 D. Demeter, T. Rousseau, P. Leriche, T. Cauchy, R. Po and J. Roncali, *Adv. Funct. Mater.*, 2011, **21**, 4379.
46 Y. S. Liu, J. Y. Zhou, X. J. Wan and Y. S. Chen, *Tetrahedron*, 2009, **65**, 5209.
47 M. Matsui, A. Ito, M. Kotani, Y. Kubota, K. Funabiki, J. Jin, T. Yoshida, H. Minoura and H. Miura, *Dyes Pigm.*, 2009, **80**, 233.
48 M. Matsui, Y. Asamura, Y. Kubota, K. Funabiki, J. Jin, T. Yoshida and H. Miura, *Tetrahedron*, 2010, **66**, 7405.
49 M. Matsui, T. Fujita, Y. Kubota, K. Funabiki, J. Jin, T. Yoshida and H. Miura, *Dyes Pigm.*, 2010, **86**, 143.
50 V. D. Mihailetchi, H. X. Xie, B. de Boer, L. J. A. Koster and P. W. M. Blom, *Adv. Funct. Mater.*, 2006, **16**, 699.
51 Y. Liang, D. Feng, Y. Wu, S.-T. Tsai, G. Li, C. Ray and L. Yu, *J. Am. Chem. Soc.*, 2009, **131**, 7792.
52 F. Würthner, T. E. Kaiser and C. R. Saha-Möller, *Angew. Chem., Int. Ed.*, 2011, **50**, 3376.
53 *Gaussian 09, Revision B.01*, Gaussian, Inc., Wallingford CT, 2010. See supporting information for full citation.
54 W. Ma, C. Yang, X. Gong, K. Lee and A. â. J. Heeger, *Adv. Funct. Mater.*, 2005, **15**, 1617.
55 G. Li, V. Shrotriya, J. Huang, Y. Yao, T. Moriarty, K. Emery and Y. Yang, *Nat. Mater.*, 2005, **4**, 864.
56 H. Jin, M. Tuomikoski, J. Hiltunen, P. l. Kopola, A. Maaninen and F. Pino, *J. Phys. Chem. C*, 2009, **113**, 16807.
57 M.-S. Kim, B.-G. Kim and J. Kim, *ACS Appl. Mater. Interfaces*, 2009, **1**, 1264.
58 J. Guo, H. Ohkita, H. Benten and S. Ito, *J. Am. Chem. Soc.*, 2009, **131**, 7792.

